Hindawi
International Journal of Aerospace Engineering
Volume 2023, Article ID 3950563, 13 pages
https://doi.org/10.1155/2023/3950563

Research Article

A New Segmented Suction Slot Design Based on the Performance of Compressor Cascade

Fengming Li, Ganchao Zhao, Lu Ye, Dongfeng Yan, and Shan Ma

College of Flight Technology, Civil Aviation Flight University of China, Sichuan, Guanghan, China

Correspondence should be addressed to Shan Ma; nirvana.shanma@gmail.com

Received 17 January 2023; Revised 20 March 2023; Accepted 18 April 2023; Published 10 May 2023

Academic Editor: Dakun Sun

To develop an effective suction slot arrangement, computational fluid dynamics simulation software and a high subsonic compressor cascade were used to simulate different suction slots. Based on the effects of various suction slots on the cascade performance under various operating conditions, a novel segmented suction slot structure Seg_3 was proposed. The results of the study revealed that in the vicinity of the operating conditions (incidence $\leq 4°$), a full-blade height suction slot should be installed at least 5% of the chord length downstream of the corner separation point to effectively remove the separation. For small and medium incidences, the best performance was observed for suction slot SS_5, which was located at 60% of the chord length downstream of the leading edge. Analyzing the effects of SS_5 and Seg_3 on the cascade performance revealed that when the incidence was less than 4°, the reductions in the total pressure loss coefficients for ζ_{suc} of SS_5 and Seg_3 both exceeded 8.2%. When the incidence was 4° or greater, the ζ_{suc} increased slightly for SS_5, whereas it decreased for Seg_3, and the ζ_{suc} was reduced. For a 3° incidence, for example, Seg_3 reduced the ζ_{suc} and passage blockage by 12.74% and 8.41%, respectively, and increased the static pressure rise coefficient by 18.55% from the baseline values. Thus, the segmented suction slot proposed in this paper outperformed conventional full-blade height suction slots.

1. Introduction

Highly-loaded compressors have attracted considerable attention for use in aeroengine designs because they can achieve high-pressure ratios. However, the flow fields inside highly-loaded compressor are complex. The 3D corner regions near the blade suction side in a highly-loaded compressor tend to accumulate low-velocity fluids. Experimental studies [1–4] have revealed that with an increase in the aerodynamic load, the axial reverse pressure gradient increases, and more low-velocity fluids accumulate; these fluids adversely affect the performance of the entire compressor stage. Therefore, eliminating accumulations of the low-velocity fluids and controlling the corner separation are critical in developing highly-loaded axial compressors.

Numerous active and passive flow control methods are used in the aerospace industry to control the performance degradation caused by airflow separation inside compressors [4–6]. Among them, boundary layer suction technology exhibits considerable advantages. This technology is typically applied to aspirate low-velocity fluids near the end wall and reduce the flow loss [7]. The technology is typically adopted in stator passages. The main types of suction technology applied in fans/compressors are holes and slots.

In 1998, the US Air Force Scientific Research Bureau carried out large-scale model verification of the suction fan at Massachusetts Institute of Technology and completed the detailed design and test of the suction fan. Since then, the suction hole has been gradually studied in the fan/compressor. Research shows that [8], as the blade blowing and suction technology is applied to tests, when the tangential speed of the high-performance fan blade tip is 450 m/s, the pressurization ratio can reach 3.4. Through the verification of tests and computer numerical simulation analysis, the boundary layer suction hole technology has achieved its expected goal. Kerrebrock et al. [9] introduced the transonic/supersonic fan stage series. As the suction hole is adopted, when the tangential speed of the blade tip is 457.2 m/s, the pressurization ratio of the rotor can reach 3.7. The paper proposed aspirated compressors and revealed

that the aspirated technology could aspirate low-velocity fluids and improve the pressurization capacity of compressors. Foreign research on the blowing/suction technology of compressor blades is based on the experimental demonstration stage, which is relatively mature.

At present, the researches on suction slots are also gradually developing. Gbadebo et al. [10] analyzed the effects of different suction slot positions on the corner region separation of the compressor blade suction surface. They revealed that these two positions exhibited strong capabilities of reducing the total pressure loss and decreasing the passage blockage. According to Gbadebo, Chen et al. [11, 12] comprehensively analyzed the effects of end-wall suction slot position on the cascade performance and concluded that the axial range of the slots should include the starting point of the corner separation. Researchers have also investigated the effect of the amount of gas suctioned by the suction slots on the cascades' performance. Gmelin et al. [13] revealed that the total pressure loss decreased with an increase in the suction flow rate, and the static pressure increased. Moreover, a suction flow ratio of 1% was adopted in most studies [14, 15], because larger suction volumes consume more external energy. Therefore, to ensure that the results of this study can be compared, with previously published results, suction slots with a suction flow ratio of 1% were used to improve the cascade performance, and the 1% suction flow rate was obtained from the plenum outlet.

Researchers have also investigated the suction slot distribution. Chen et al. [12] proposed a segmented end-wall suction slot design. The authors believed that the formation of the three-dimensional corner separation in cascades is produced by the confluence of the suction side branch of the horseshoe vortex and the pressure surface branch of the adjacent blade in the blade passage. This phenomenon occurs under the pitch pressure gradient under the blade suction side/end-wall corner region. Based on the horseshoe vortex formation process, a segmented suction slot design was proposed. Studies have revealed that this design can reduce the total pressure loss in a cascade by 11.2% and increase the static pressure by 9.84%. Ma et al. [16] proposed a novel segmented suction slot design for blade suction sides and revealed that with increases in the incidence, the corner separation range near the suction side gradually expands along the span and chord directions. Furthermore, the separation point also continues to move forward, and before a stall occurs, this separation range always includes the corner region formed by the end-wall and the blade's trailing edge. They then proposed a segmented suction scheme for the blade suction side. The study revealed that this design could increase the cascade stall incidence from 8° to 10°.

This study considered a high subsonic cascade, and the correlation between the position of the suction slot and the corner separation in the compressor cascade was discussed. A superior segmented suction slot design was proposed based on the performance characteristics of a suction slot with a full-blade height. This study achieved three primary objectives:

(1) A quantitative method was proposed to express the relationship between the corner separation point and the suction slot. Relationships between the optimal positions of the suction slots and the separation point were discussed for a variety of operating conditions

(2) The effects of the axial position of the suction slot on the cascade performance were analyzed for various incidences, and suggestions regarding the axial placement of the suction slot were provided

(3) A segmented suction slot design for the blade suction side that was based on the performance of a suction slot with a full-blade height was proposed

2. Axial Compressor Cascade and Suction Methods

A subsonic axial compressor cascade was used during this study. The cascade profile was derived from the NACA-65 K48 airfoil [11]. Chen et al. [11, 12] conducted aerodynamic experiments with the baseline using oil flow visualization technology in the high subsonic cascade experimental wind tunnel at the Institute of Propulsion Technology in the German Aerospace Center. The inlet of the wind tunnel was connected to a 40 mm (width) × 90 mm (length) rectangular nozzle. The contraction ratio of the nozzle was 1 : 218, so the Mach number (Ma) of the cascade inflow could be accelerated to 0.7. The detailed aerodynamic and geometric parameters are presented in Section 2.1.

2.1. Compressor Cascade. The cascade had a designed Mach number of 0.67 and a Reynolds number of 560,000. Table 1 presents the actual geometric dimensions and the primary aerodynamic parameters used in the experiment. The parameters in the table are illustrated in Figure 1, which depicts the two-dimensional arrangement and crucial geometric and aerodynamic parameters. In the figure, t represents the pitch, LE is the blade's leading edge, and TE is the trailing edge. The measurement cross-section in the experiment was located 0.4 C downstream of the TE.

2.2. Introduction of the Suction Slot. At a large incidence, the boundary layer of the inner end wall of the cascade passage is pushed to the blade suction side under the high transverse pressure gradient, and a flow separation is formed in the corner region. Opening suction slots on the suction side of the blade can absorb the accumulated low-velocity fluids near the slots, which improves the flow field performance.

A full-blade height suction slot was investigated during this study. Figures 2 and 3 display schematics of the cascade with a slot. Figure 2 displays a 3D geometric model of the cascade with a suction slot and a plenum chamber. To simulate the actual nonuniform suction of the suction slot, actual suction blades were simulated inside the blades, and a plenum chamber was established. To ensure that the flow at the outlet of the plenum chamber did not affect the flow between the suction slot and the blade suction side, the length of the plenum outlet was extended to 0.5 h.

Figure 3 presents a two-dimensional schematic of the suction cascade. This study investigated the effects of

Table 1: Geometric and aerodynamic parameters of the compressor cascade [11].

Parameter	Value
Inflow Mach number (Ma)	0.67
Inlet airflow angle (β_1)	132°
Outlet airflow angle (β_2)	90°
Mounting angle (γ)	112.5°
Blade chord length (C)	40 mm
Full-blade height (h)	40 mm
Pitch (t)	22 mm

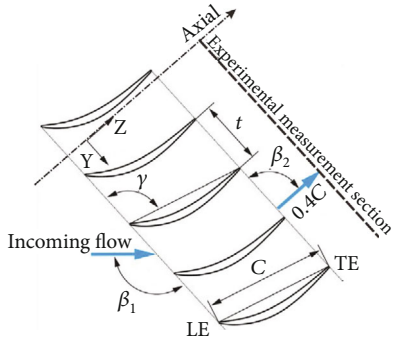

Figure 1: Schematic of the two-dimensional cascade geometry [17].

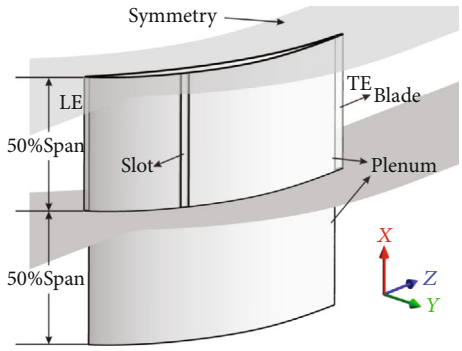

Figure 2: Three-dimensional schematic of the cascade with a suction slot.

different positions of the spanwise suction slot on the cascade performance. Therefore, the axial distance, Z_{SS} (along the z-axis, with SS representing the suction slot), from the center point (red dot in Figure 3) of the spanwise slot to the LE was used to describe the position of the suction slot. The width of the suction slot is represented by W_{SS} (W denotes width). In this study, $W_{SS} = 0.01\,C$.

3. Numerical Simulation Method

3.1. Computational Domain and Boundary Conditions. The commercial software ANSYS CFX was used to perform numerical simulations. The IGG-Autogrid5 generated the calculation mesh. The calculation domain, boundary conditions, and meshing method are displayed in Figure 4. Considering that the blades of the axial compressor cascade were vertically symmetric, half of the blade was generated in the computational domain to reduce the computation costs. The solid wall in the flow field was defined as a no-slip boundary, while the upper surfaces of the passage, the suction slot, and the plenum chamber were defined as symmetry boundaries. The inlet was a total pressure boundary. The incidence was adjusted by changing the airflow angle. The static pressure at the outlet was set to 101325 Pa. To ensure that the outlet airflow was fully mixed, the outlet boundary was extended to 250% of the axial chord length downstream of the TE. The outlet of the plenum chamber was defined as a static pressure boundary. The suction flow was changed by adjusting static pressure, and a translation period was used for the periodic boundary.

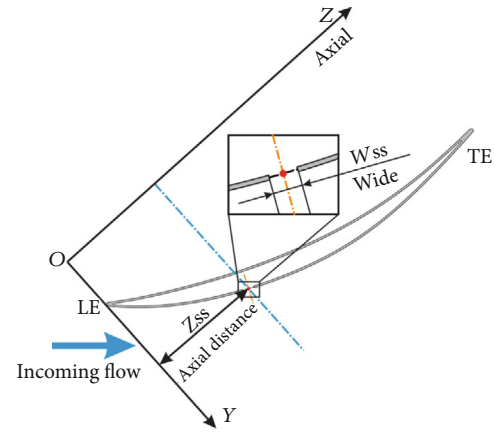

Figure 3: Two-dimensional top view of the suction slot.

To ensure that the $Y+$ value was less than 1, the element height of the first layer was set to 1e-6 m. The mesh had an expansion ratio in the boundary layer of 1.1, and the nodes were 33. To ensure the mesh quality, an O-shaped topology was used around the blade. To accurately capture the flow field, the LE and TE were densified. To ensure the grid quality and calculation accuracy, a butterfly topology was used for meshing inside the plenum chamber, and the mesh was locally densified around the suction slot. The locally adjusted mesh portions are presented in the enlarged views within Figure 4.

3.2. Mesh and Numerical Model Verification. The authors referred to the numerical simulations from Chen et al. [12] for the cascade parameters, and the SST k–ω model was used as the turbulence model. Grid independence verification is critical for ensuring the accuracy of results while conserving computing resources. In this study, eight sets of meshes were used for verification. The mesh set with the minimum number of nodes had 0.54 million nodes. The number of nodes increased along three directions (the meshes in the boundary layer were fixed). The increase in the number of nodes for each successive mesh was guaranteed to be approximately 600,000 (O-shaped meshes surrounded the blades, so achieving the same number was difficult). The final numbers of nodes were 0.54 million, 1 million, 1.63 million, 2.42 million, 2.98 million, 3.45 million, 3.91 million, and 4.43

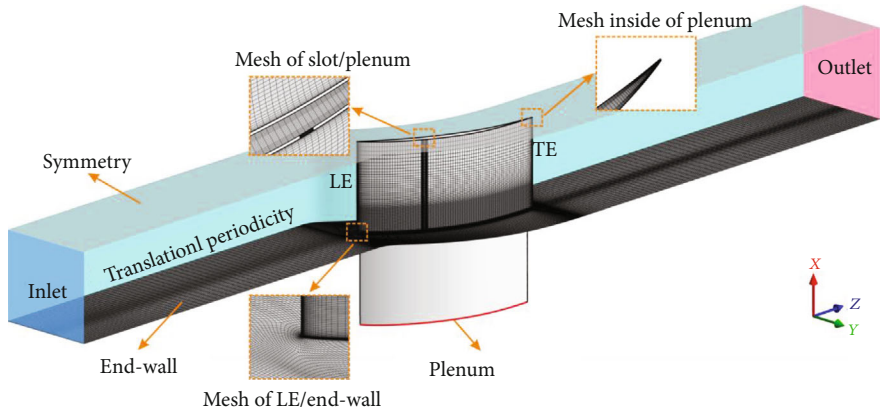

Figure 4: Computational domains and meshes.

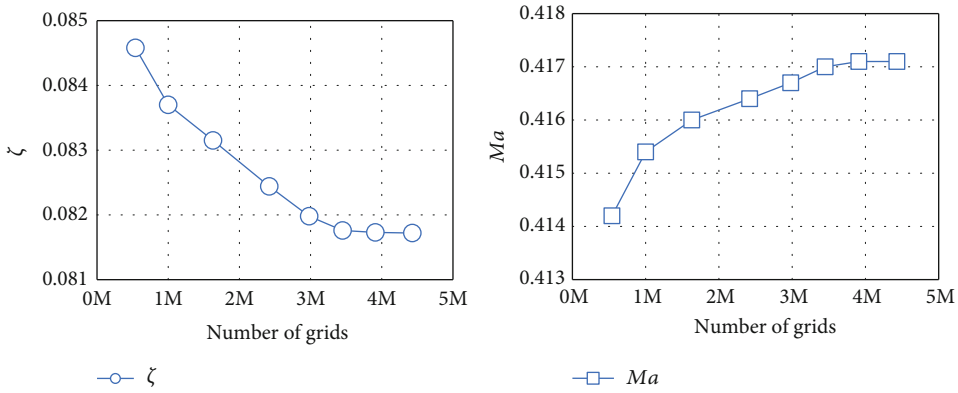

Figure 5: Variations in ζ and Ma with the number of nodes at the measurement cross-section.

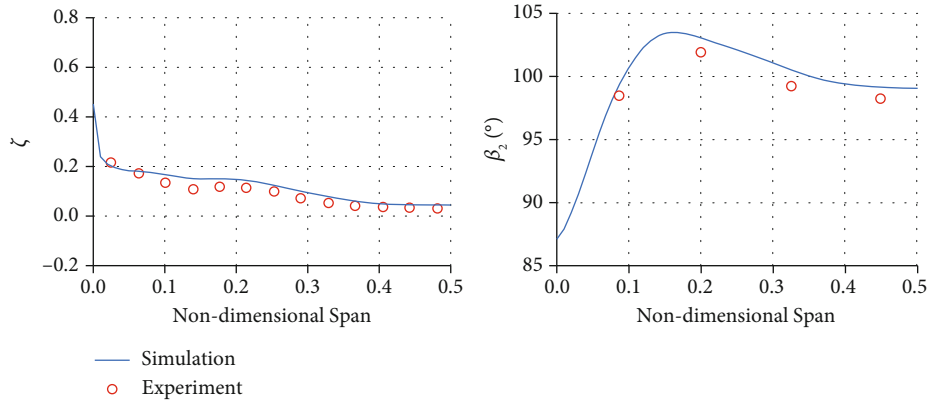

Figure 6: Comparisons between the numerical simulation results and the experimental results.

million. The mass flow average total pressure loss coefficient ζ and the Ma were extracted at the measurement cross-section (40% of the axial chord length downstream of the TE) for the different mesh sets. The changes in ζ and Ma with changes in the numbers of nodes are displayed in Figure 5, which reveals that with increases in the number of nodes, ζ decreased gradually, and Ma increased gradually. For more than 3.45 million nodes, the values of ζ and Ma remained nearly unchanged. Thus, increasing the number of nodes past 3.45 million had only a limited effect on the cascade performance. Therefore, 3.45 million nodes (half-blade height) were used in the subsequent simulations. The ζ is a crucial parameter that represents the performance of the compressor cascade. It is defined by

$$\zeta(x, y, z) = \frac{\mathrm{Pt}_{\mathrm{in}} - \mathrm{Pt}(x, y, z)}{\mathrm{Pt}_{\mathrm{in}} - P_{\mathrm{in}}}, \tag{1}$$

where Pt is the total pressure, P is the static pressure, the subscript in represents the inlet cross-section, and (x, y, z) represents the set of local parameters.

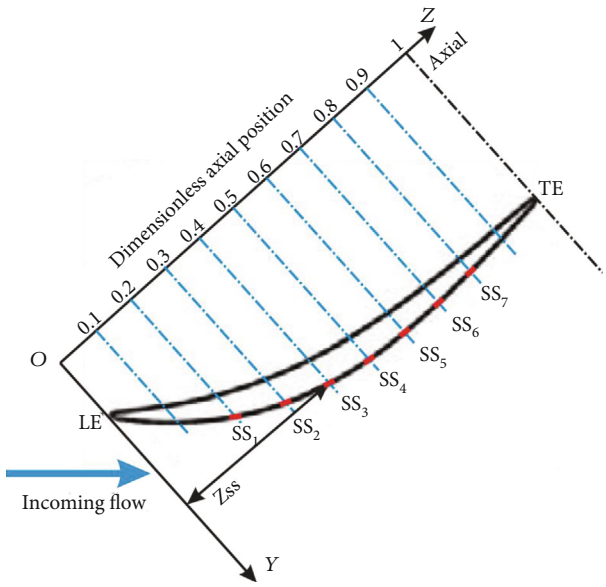

Figure 7: Suction slot design.

Figure 6 presents comparisons between the numerical calculation results and the experimental data to verify the reliability of the numerical simulation method. The abscissae in the plots are both the dimensionless blade height, while ζ is in the left plot, and the outlet airflow angle is the β_2 in the right plot. The comparisons reveal that the flow loss could be captured by the simulations, especially its variations trend along the blade height direction. The loss was only slightly underestimated in the area near the cascade wall, which could be attributed to measurement errors in the flow field near the end wall during the experiments. Furthermore, the predications of the outlet airflow angle trend in the blade height direction were highly accurate, with only a slight overall overestimation, which had a limited effect on the flow performance estimations. Therefore, the numerical simulation methods were feasible for this study.

4. Analysis of the Simulation Results

4.1. Introduction of the Suction Scheme. Using boundary layer suction technology on the suction side of a blade can effectively absorb the low-velocity fluids near the walls [17, 18]. Studies have revealed that the axial positions of a suction slot considerably affect the flow loss reduction in a cascade [17]. However, limited quantitative studies have been conducted regarding the effects of the axial positions of suction slots on the aerodynamic performance of the cascade. In this study, a correlation was established between the axial position of the suction slot on the blade suction surface and the total pressure loss.

First, a design scheme for the suction slot was developed. Figure 7 displays a cross-sectional view of the cascade. Because both edges of the blade were thin, making a slot there takes work. The axial positions of the seven suction slots in the figure were set sequentially in the Z direction. The z-axis represents the dimensionless axial distance in the cascade. The dimensionless axial chord length was equal

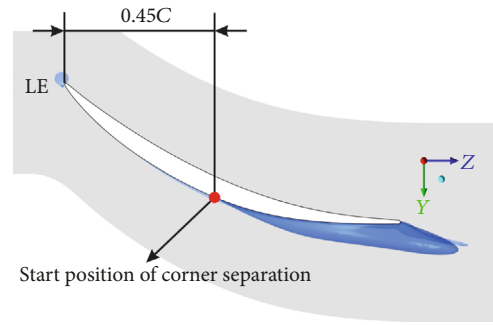

Figure 8: Three-dimensional corner separation under the 0° incidence design condition.

Table 2: Axial positions of the suction slots with respect to the separation point of the associated corner region.

Suction slot	SS_1	SS_2	SS_3	SS_4	SS_5	SS_6	SS_7
Z_{SSi}	−0.25	−0.15	−0.05	0.05	0.15	0.25	0.35

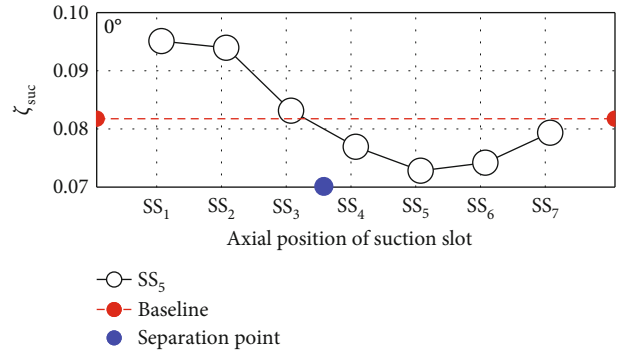

Figure 9: Relationship between ζ_{suc} and the suction slot positions (at a 0° incidence).

to 1. The distances between the suction slots and the y-axis ranged from 0.2 to 0.8. The spacing between the slots was 0.1. The seven slots (marked in red in Figure 7), which were named SS_1–SS_7, started from an axial position of 0.2. As displayed in Figure 7, the axial distance between SS_1 and the y-axis was 0.2 C, and the axial distance from SS_2 to the y-axis was 0.3 C, the distances between the rest of the slots and the y-axis followed this pattern as well.

Part of the air flowed out from the suction slots when the boundary layer suction technology was used, so the effects of the suction slots should be considered. When calculating the total pressure loss of a cascade with suction slots, the corrected total pressure loss coefficient ζ_{suc} can be used:

$$\zeta_{suc} = \frac{(1\text{-}\dot{m}) \cdot (Pt_{in} - Pt_{out}) + \dot{m} \cdot (Pt_{in} - Pt_{ple})}{Pt_{in} - P_{in}}. \quad (2)$$

In Equation (2), subscript ple denotes the outlet of the blade plenum chamber, subscript in is the inlet section of the blade passage, and subscript out is the outlet section of

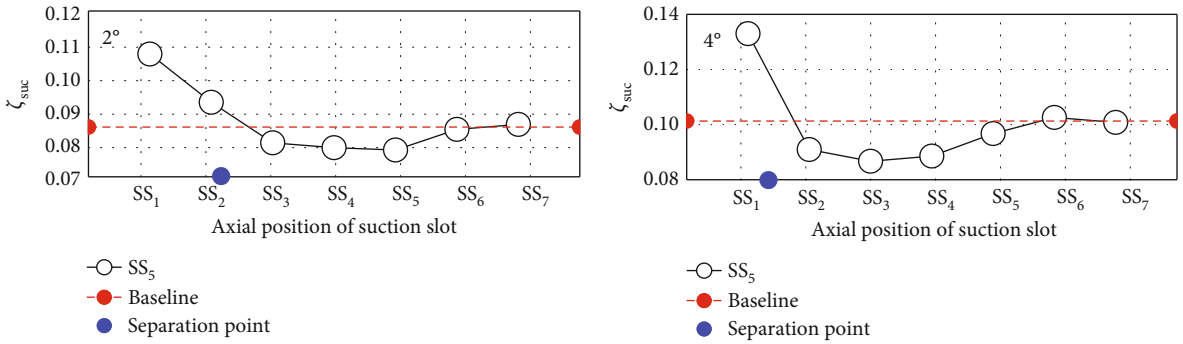

(a) 2° incidence (b) 4° incidence

Figure 10: Relationships between ζ_{suc} and the suction slot position.

the blade passage. The $\dot{m}$ is the mass flow rate at the outlet of the plenum chamber, which could be obtained by dividing the flow rate at the outlet of the plenum chamber by the cross-sectional area of the flow field passage inlet. The readers should note that when this paper refers to the total pressure loss coefficient, the coefficient for a baseline cascade without suction slots is denoted by ζ, while that for the cascade with a suction slot is denoted by ζ_{suc}.

To obtain a correlation between the slot positions and the corner separation, the axial position coefficient Z_{SSi} was used to describe the axial positions of the slots according to

$$Z_{SSi} = \frac{Z_{SS} - Z_{CS}}{C}. \quad (3)$$

In Equation (3), Z_{CS} represents the distance between the starting point of the 3D corner separation region and the LE of the cascade under the corresponding operating conditions, and the value of subscript i represents the different suction slots. Z_{CS} is equal to 0.45 C under the 0° incidence design condition, as displayed in Figure 8.

As presented in Table 2, suction slots with negative axial position were located upstream of the starting position of the corner separation, while the other slots were located downstream of the starting position. For example, the negative value associated with SS_1 indicates that this slot was located upstream of the starting position of the corner separation and that its axial distance to the separation point was 0.25 C.

4.2. Performance Analysis of the Full-Blade Height Suction Slots. Figure 9 displays the effects of the suction slots at various axial positions on the ζ_{suc} of the cascade under the 0° incidence design condition. The red dashed line represents the ζ_{suc} of the baseline, and the black mark represents the ζ_{suc} for the cascade with different suction slots. The blue dot in the figure represents the starting position of the corner separation region in the baseline. The values of ζ_{suc} in Figures 9–11 are all the average mass flow rates measured at the outlet cross-section and are expressed by

$$\frac{\int \zeta_{suc} d\dot{m}}{\dot{m}}. \quad (4)$$

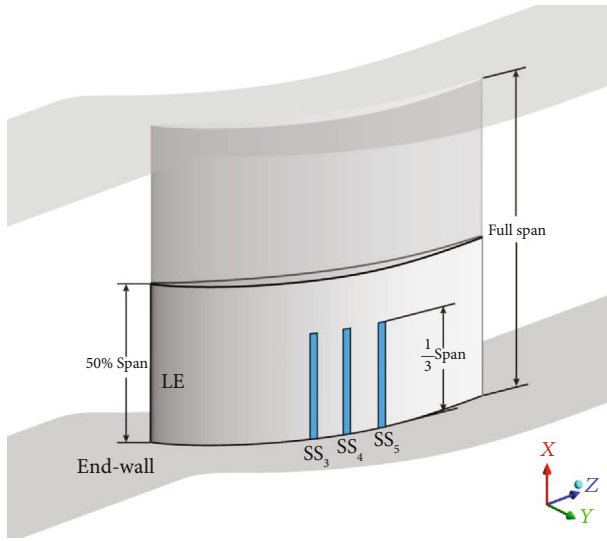

Figure 11: Schematic of the segmented suction slot structure.

The figures reveal that as the suction slot axial position changed from near the LE of the blade (SS_1) to near the TE of the blade (SS_7), the ζ_{suc} changes changed considerably, first increasing and then decreasing. For the suction slots that were upstream of the separation point of the corner separation, that is, SS_1-SS_3, the ζ_{suc} was greater than the baseline value (the red dashed line), and the cascade performance was adversely affected. For the suction slots that were downstream of the starting position of the corner separation, that is, SS_4–SS_7, the ζ_{suc} was less than the baseline value (the red dashed line). It first decreased and then increased, and its optimal location was at SS_5.

The results discussed above led to certain conclusions. First, the axial position of the full-span suction slot considerably affected the total pressure loss of the cascade. When the suction slot was located upstream of the separation point of the baseline, it adversely affected the performance of the cascade, leading to an increase in the ζ_{suc}. According to Table 2, when a slot is located at 0.05 C downstream of the separation point of the baseline (SS_4, or $Z_{SS0} = 0.05$) under the design conditions, the ζ_{suc} begins to decrease. The minimum value of the total pressure loss

was reached at SS_5 ($Z_{SS0} = 0.15$). At this location, the ζ_{suc} was reduced by 10.9%.

To explain these conclusions, it was critical to analyze the flow field. Figure 12 presents a comparison between the 3D flow fields of the baseline, the cascade with SS_1, and the cascade with SS_5 under the 0° incidence design condition. SS_1 and SS_5 are the two typical cases that had the largest and smallest total pressure losses, respectively. In the figure, a red line marks a suction slot on the blade suction side, and the limit streamlines are displayed on the wall. The extraction value of the blue three-dimensional iso-value surface is $v_z = -0.0001$ m/s, which indicates that the airflow velocity within the range wrapped by the iso-value surface was negative along the z-axis, that is, the airflow through the iso-value surface was backflow, representing the airflow separation region. The contour of the ζ was extracted for the cross-section at 40% of the chord length downstream of the TE.

As shown in Figure 12(a), the starting position of the airflow separation in the baseline appeared at a distance equal to 45% of the chord length downstream of the LE. The flow field can be improved if the suction slots can absorb part of the separated gas. As displayed in Figure 12(b), when a suction slot on the blade suction side was located at a distance equal to 20% of the chord length downstream of the LE (SS_1), the three-dimensional flow separation area increased, typically along the z-axis, and the total pressure loss on the downstream portion of the blade also increased considerably.

Figure 12(c) shows that when the suction slot was located at 60% of the chord length downstream of the LE, the 3D corner separation region become considerably smaller in the Z direction. The contour of the ζ on the downstream portion of the blade reveals that the pressure loss decreased and that the size of the high-loss area also decreased. These phenomena are crucial to improving the cascade performance.

The results discussed above also led to multiple conclusions. Suppose the suction slots are located upstream, far away from the separation point of the baseline. In that case, the airflow from the downstream part of the suction slot is sucked upstream, which causes significant backflow and intensifies the airflow separation. When the suction slot was located at a suitable position downstream of the separation point of the baseline, not only did the separation associated with the upstream suction slots nearly disappear, but the size of the airflow separation region downstream as well as the total pressure decreased.

To illustrate the relationship between the axial suction slot position and the corner separation, the effects of placing the suction slot at various axial positions on the ζ of the cascade were analyzed for 2° and 4° incidences. Figure 13 reveals that the starting positions of the 3D corner separation in the baseline for the 2° and 4° angles of attack were located at 32% and 15% of the chord length downstream of the LE, respectively.

Figure 10 displays the effects of placing the suction slot at various axial positions on the ζ_{suc} of the cascade at incidences of both 2° and 4°, respectively. The labels in the figure are the same as those in Figure 9. Figure 10(a) reveals that when the incidence was 2°, as the axial position of the suction slot moved from SS_1 to SS_7, the ζ_{suc} first decreased and then increased, and it reached a minimum value at SS_5, which result is consistent with that for the 0° incidence. However, when the suction slot moved backward to SS_3, the ζ_{suc} decreased to a value smaller than that of the baseline. This phenomenon can be attributed to the fact that for a 2° incidence, the starting position of the corner separation of the baseline moved forward to the blue dot, as displayed in Figure 10(a). At this stage, the ζ_{suc} decreased because the suction slot SS_3 was located behind the separation point. This situation also occurred for the 4° operating condition, as displayed in Figure 10(b). As the axial installation position of the slot moved from SS_1 to SS_7, the ζ_{suc} first decreased and then increased. Unlike for the 0° and 2° incidence, the ζ_{suc} reached the lowest value at SS_3. The total pressure loss decreased below the reference value when the suction slot was located at SS_2, just downstream of the reference corner separation point. This phenomenon confirms that when the suction slot was located downstream of the separation point in the baseline, the ζ_{suc} tended to decrease.

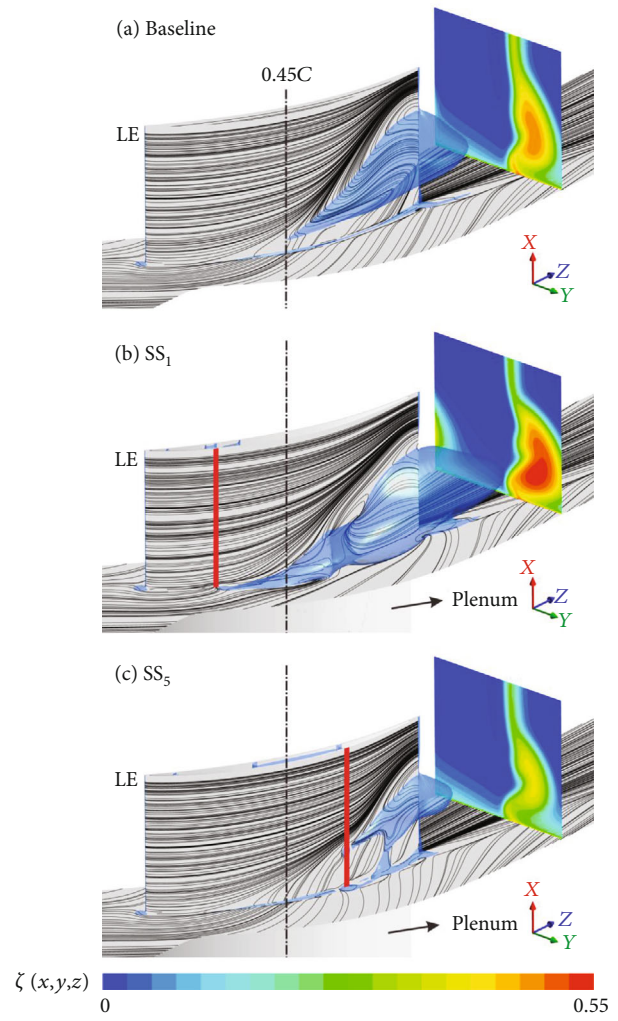

Figure 12: Effects of typical axial positions of suction slots on the cascade performance.

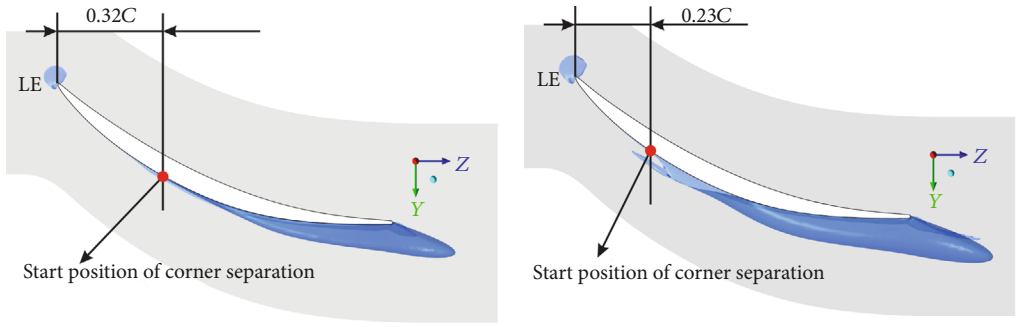

(a) 2° incidence (b) 4° incidence

Figure 13: Three-dimensional corner separation at typical incidences.

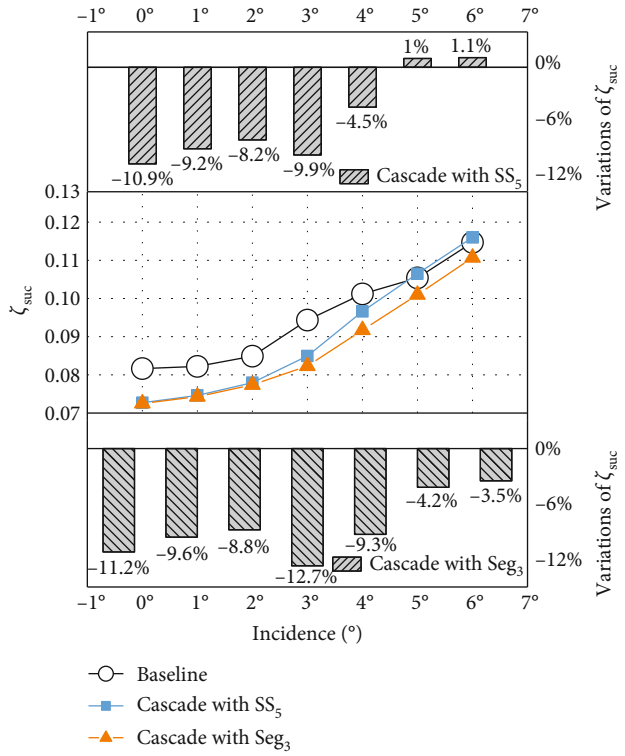

Figure 14: Effects of the suction slot under various operating conditions.

Conclusions could also be drawn from the previous discussion. At 2° and 4° incidences, when the slot was located downstream of the separation point of the baseline, and the axial distance from the separation point was 0.08 C and 0.07 C (i.e., $Z_{SS2} = 0.08$ and $Z_{SS4} = 0.07$), the ζ_{suc} exhibited a decreasing trend. When the incidence was 2° and 4°, the suction slots with the most significant decrease in the ζ_{suc} are suction slots that were SS_5 and SS_3 ($Z_{SS2} = 0.28$, $Z_{SS4} = 0.17$), which had pressure loss reductions of 8.15% and 14.41%, respectively. Suction slots SS_3, SS_4, and SS_5 exhibited certain advantages in reducing the total pressure loss of the cascade at 2° and 4° incidences. SS_4 and SS_5 considerably reduced the ζ_{suc} of the cascade at a 0° incidence.

The following segmented suction slot comprehensively considers the suction slot location advantages under several typical operating conditions. The advantages and characteristics of this type of structure are also discussed.

4.3. Performance Analysis of the Segmented Suction Slots. Figure 11 displays a schematic of the segmented suction slot on the blade suction side. To make the segmented suction slot comparable to the full-blade height suction slot, segments that were 33% of the blade height were placed at the original positions of SS_3, SS_4, and SS_5. The sum of the areas of the three cross-sections was equal to the cross-sectional area of the full-blade height suction slot. The suction flow rate on the outlet of the plenum was 1%. The study object when using the segmented suction slot was named Seg_3 (i.e., segmented suction with three slots). Figure 11 displays a schematic of the full-blade single-passage cascade. These

settings were only intended to make the segmented suction slot intuitive. The calculation domain was still the single-passage half-blade height flow field, and the symmetry boundary condition was set for the 50% span.

Figure 14 presents the effects of suction slots SS_5 and Seg_3 on the total pressure loss at incidences of 0°–6° incidences. The upper portion of the figure shows the variations in the ζ_{suc} for SS_5, the middle portion presents the values of the ζ_{suc}, and the lower portion depicts the variations in the ζ_{suc} for Seg_3. At minor incidences ($i < 3\circ$), SS_5 and Seg_3 both exhibited considerable abilities to reduce the total pressure loss, especially at the designed operating condition (0° incidence) and at 3° incidence. For 0° and 3° incidence, SS_5 reduced the ζ_{suc} by 10.9% and 9.9%, respectively, and Seg_3 reduced the ζ_{suc} by 11.2% and 12.7%, respectively, with respect to the baseline values.

At incidences with less than 4°, the reductions in the total pressure loss for SS_5 and Seg_3 exceeded 8.2%, which represents a significant reduction. At incidences $\geq 4\circ$, the reductions in the ζ_{suc} were small, and the ζ_{suc} for SS_5 actually increased slightly. Seg_3 reduced the ζ_{suc} slightly at large incidences. Multiple conclusions could be drawn from the results discussed above.

At medium and small incidences, full-blade height suction slot SS_5, which was located downstream of the separation point of baseline's separation point, could reduce the cascade's total pressure loss. The segmented suction slot Seg_3 was proposed after considering that an appropriate selection of the suction slot position exhibited an excellent capability for improving the cascade performance. At large incidences, SS_5 did not improve the performance of the cascade. However, Seg_3 could reduce the total pressure loss in the cascade for large incidence. To further analyze the change of flow field characteristics, the details of three-dimensional flow fields at high incidences are given in Figures 15 and 16.

It is difficult to judge the stall condition of the cascade and the effect of the suction slot on the cascade performance only through the changed total pressure loss coefficient. Therefore, Figures 15 and 16 show the three-dimensional flow fields of the baseline cascade and the cascades with the SS_5, and Seg_3 at 6° and 7° incidences to analyze the effects of the suction slot on the stall characteristics. The blue three-dimensional iso-value surface indicates the airflow separation area. The contour of the ζ is extracted at a cross-section at 40% of the chord length downstream of the TE.

According to Figure 15, when the incidence increases to 6°, the suction slot does not significantly improve the accumulation of low-energy fluid. The total pressure loss on the downstream section of the blade's trailing edge changes little, which indicates that the suction slots with different structures (SS_5 and Seg3) have a weak ability to remove an extensive range of low-energy fluid. When the incidence increases to 7°, the low-energy fluid in the baseline increases sharply, and the total pressure loss increases significantly. The flow field suddenly deteriorated at this time, indicating that the corner stall had occurred. For Figures 16(b) and 16(c), the full-blade high suction slot and segmented suction slot did not delay the occurrence of corner stall, and the sudden increase of separation

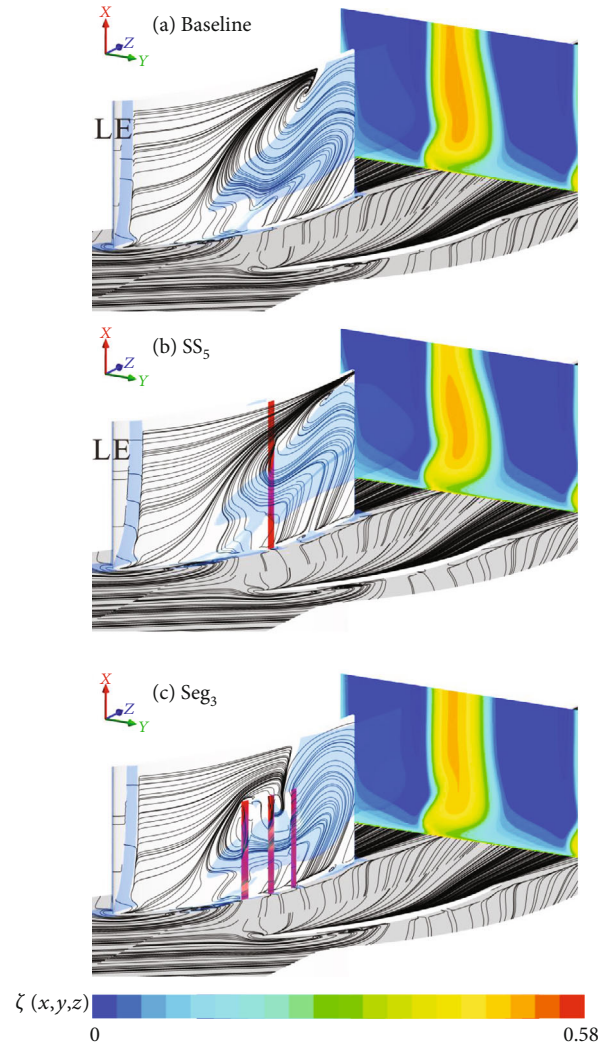

Figure 15: Three-dimensional flow fields of the baseline, SS_5, and Seg_3 at 6° incidence.

area and the sharp increase of total pressure loss still occurred at the 7° incidence. Therefore, these two suction slots could not effectively improve the stall characteristic.

To discuss the performance advantages of segmented suction slot Seg_3, which was proposed after considering the effects of suction slot position, the compressor performance was quantitatively analyzed using multiple parameters, including the static pressure rise coefficient, the total pressure loss coefficient, and the blockage.

The static pressure rise coefficient is a critical parameter for evaluating compressor performance. It reflects the capability of the cascade and stator to increase the static pressure, expressed by C_p, according to

$$C_p(x, y, z) = \frac{P(x, y, z) - P_{in}}{Pt_{in} - P_{in}}. \quad (5)$$

The blockage evaluation method proposed by Khalid [19] was used to obtain the blockage distribution in the

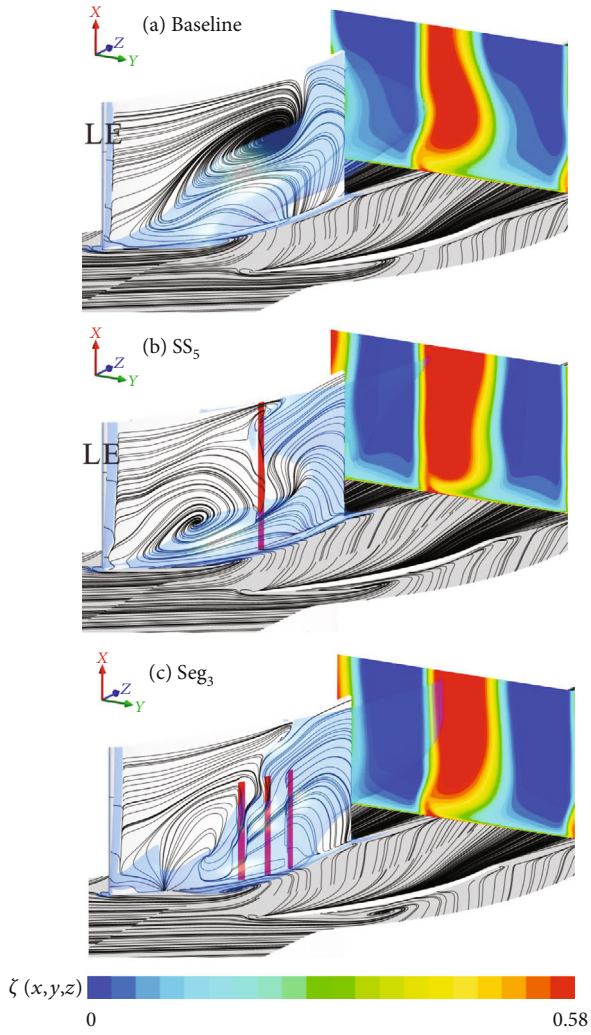

Figure 16: Three-dimensional flow fields of the baseline, SS_5, and Seg_3 at 7° incidence.

cascade passages. He proposed using the scalar $\nabla(\rho v_m)$ to evaluate the blockage; however, the local blockage boundary should be reflected on the plane perpendicular to the axial direction. Therefore, the gradient magnitude should be obtained from the gradient components of $\nabla(\rho v_m)$ on the axial plane in the span and circumferential directions. For a Cartesian coordinate system, this gradient can be expressed as $|\nabla(\rho vm)|_{x,y}$. Khalid revealed that after the blockage equation has been nondimensionalized, the contours equal to two are defined as the blockage boundary. The area with contours more significant than two is the blockage area. After nondimensionalization, the blockage boundary in this study was defined by

$$\frac{|\nabla[\rho v_m]|_{x,y}}{(\rho_{\text{in}} v_{\text{in},C}/C)} = 2, \tag{6}$$

where ρ_{in} represents the average density at the inlet cross-section, v_m is the velocity component of the airflow in the primary flow direction, and $v_{\text{in},C}$ is the average axial velocity at the inlet cross-section.

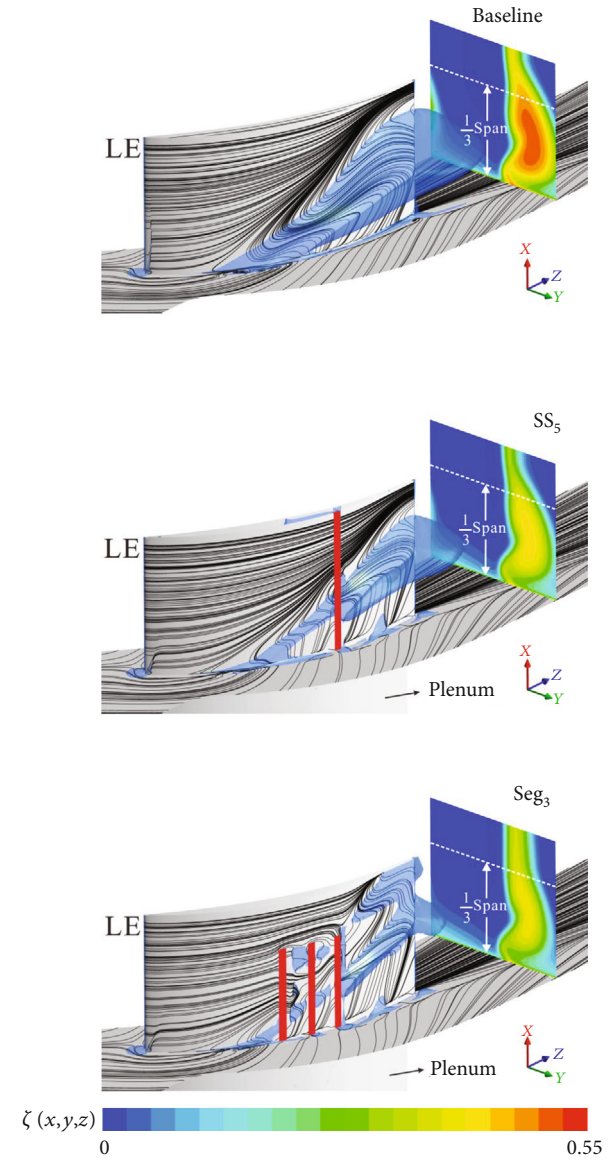

Figure 17: Three-dimensional flow fields of the baseline cascade and cascades with SS_5 and Seg_3 at 3° incidence.

The blockage area in the passage cross-section at the TE is represented by A_{blo}, which denotes the extent of the blockage of the flow field passage.

Figure 17 displays a comparison between the flow fields of the baseline cascade and the cascades with SS_5 and Seg_3 at 3° incidence. In each image, the airflow in the blue three-dimensional iso-surface is the backflow, which represents the airflow separation area. A cross-section at 40% of the chord length downstream of the TE was considered. The contour of the ζ was extracted at this position. The passage blockage at the TE cross-section is represented by a gray area in Figure 18, where SS represents the suction side and PS represents the pressure surface. Table 3 summarizes the performance parameters of the three cases, which are used

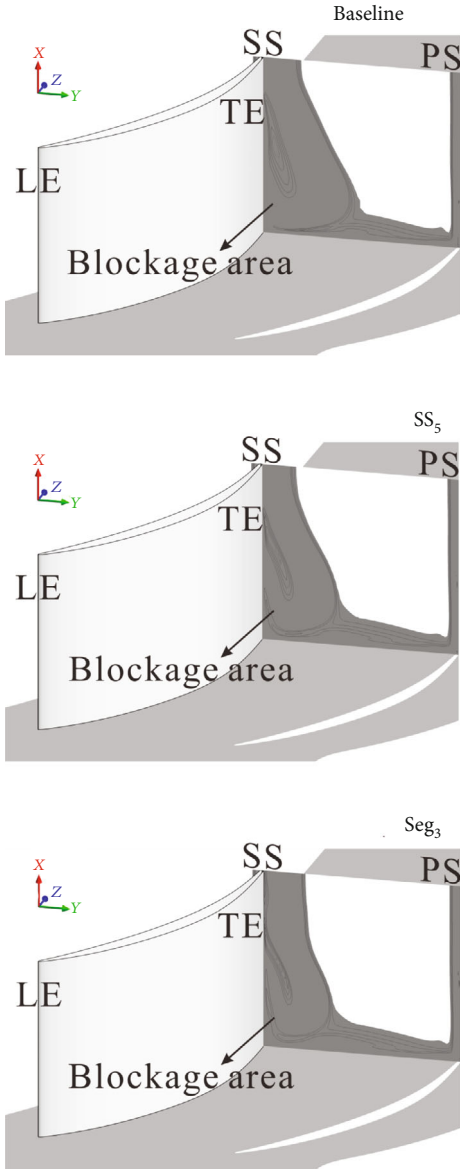

Figure 18: The passage blockage at the TE cross-section.

Table 3: Performance parameters of the baseline cascade and cascades with SS_5 and Seg_3.

Case	ζ_{suc}	C_p	A_{blo} (cm^2)
Baseline	0.09445	0.4678	2.033
SS_5	0.08505	0.5426	1.893
Seg_3	0.08242	0.5546	1.862

to analyze the cascade performance from Figure 17. Here, ζ represents the mass flow rate's average total pressure loss coefficient as expressed in Equation (4). Furthermore, C_p represents the average static pressure rise coefficient of the mass flow rate and is expressed by

$$\frac{\int C_p d\dot{m}}{\dot{m}}. \quad (7)$$

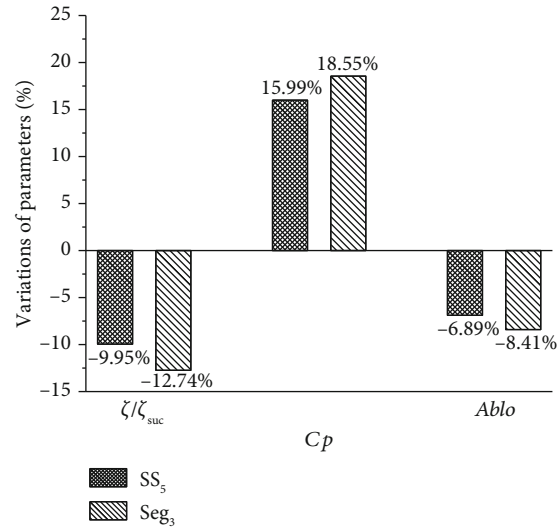

Figure 19: Three performance parameters of cascades with SS_5 and Seg_3 relative to the baseline cascade.

The bar graph in Figure 19 reveals the variations in the three performance parameters, ζ_{suc}, C_p, and A_{blo}, for cascades with SS_5 and Seg_3 relative to the baseline values and based on Table 3.

Figure 17 reveals that the 3D corner separation was effectively reduced from that of the baseline cascade because of the effect of full-blade height suction slot SS_5, especially since the separation upstream of the slot almost disappeared. The contour of the ζ and the blockage (Figure 18) reveals that the high loss in the core area of the total pressure loss decreased significantly and that the range of the maximum blockage in the pitch direction in the passage also decreased. Finally, with respect to the baseline values, ζ_{suc} was reduced by 9.95%, the passage blockage was reduced by 6.89%, and the static pressure rise coefficient increased by 15.99% (Figure 19).

Figure 17 reveals that the separation region decreased more for Seg_3 than for SS_5. The separation nearly disappeared within a distance equal to one-third of the blade span height from the end wall; this result can be attributed to the suction slot distribution characteristics. Although additional separations occurred near the middle of the blade span, the overall flow loss decreased considerably, especially the high flow loss in the core area of the total pressure loss. The range of the maximum blockage in the pitch direction in the passage also decreased markedly. Finally, with respect to the baseline values, the ζ_{suc} was reduced by 12.74%, the passage blockage was reduced by 8.41%, and the static pressure rise coefficient increased by 18.55% (Figure 19).

5. Conclusions

A high subsonic cascade was used as a case study to comprehensively investigate the effects of changing the axial position of a full-blade height suction slot on the cascade performance. The optimal axial position of the slot was quantitatively analyzed using the starting position in a

corner region separation of the baseline cascade as a reference. The study produced three primary conclusions:

(1) At medium and small incidences, as the axial position of the slot changed from the front to the back of the blade surface, the total pressure loss first decreased and then increased. At 0° and 2° incidences, the optimal location of the suction slot was 60% of the chord length downstream of the LE (SS_5). Placing a suction slot at this location reduced the total pressure loss coefficient (ζ_{suc}) for the 0° and 2° incidences by 10.9% and 8.2%, respectively, from the baseline values. For a 4° incidence, the optimal location of the suction slot was 50% of the chord length downstream of the LE (SS_4); placing the suction slot at this location reduced the ζ_{suc} by 14.41% from the baseline value

(2) The relationship between the location of a slot and the corner separation point at different working conditions was also investigated. At incidences of 0°, 2°, and 4°, when the suction slot was located downstream of the separation point of the baseline cascade, ζ_{suc} decreased with $Z_{SS0} = 0.05$, $Z_{SS2} = 0.08$, and $Z_{SS4} = 0.07$, respectively, and reached minimum values at $Z_{SS0} = 0.15$, $Z_{SS2} = 0.28$, and $Z_{SS4} = 0.17$, respectively. At medium and small incidences, a full-blade height suction slot should be installed downstream of the corner separation point to achieve desired results. The slot should be located at least 0.05 C downstream of the separation point to consider the effects of various operating conditions. For the best performance, the full-blade height suction slot should be installed between 0.15 C and 0.28 C downstream of the corner separation point

(3) Based on the effect of the axial position of the full-blade height suction slot on the cascade performance, a segmented suction slot Seg_3 was proposed. Comparisons between Seg_3 and SS_5 revealed that when the incidence was less than 4°, the ζ_{suc} reductions were more than 8.2% for both SS_5 and Seg_3. When the incidence was 4° or greater, the reduction in ζ_{suc} was slight, ζ_{suc} increased slightly for SS_5, and Seg_3 reduced ζ_{suc} slightly at large incidences. For an incidence of 3°, SS_5 could reduce ζ_{suc} by 9.95% and the passage blockage by 6.89% from the baseline values, and it could increase the static pressure rise coefficient C_p by 15.99% from the baseline value. However, because of its distribution characteristics, Seg_3 could nearly eliminate the separation within a distance equal to one-third of the blade span from the end wall. Therefore, ζ_{suc} and the passage blockage were reduced by 12.74% and 8.41%, respectively, and the C_p increased by 18.55% from the baseline values

These nondimensional analysis results can be used to establish a standardized guide for the selection of the suction slot axial position. When designing suction slots for other axial compressor cascades, finding the position of the corresponding separation point for the same operating condition is necessary. The suction slot position can be then estimated using Conclusion 2. The conclusions of this study should be verified theoretically using numerous cascade models.

Data Availability

The data are available on request from the authors. The data that support the findings of this study are available from the corresponding author upon reasonable request.

Conflicts of Interest

The authors declare that they have no conflicts of interest.

Acknowledgments

This research was funded by the Sichuan Natural Science Foundation for Distinguished Young Scholars (through grant no. 23NSFSC2925), by the Key Laboratory of Flight Techniques and Flight Safety, CAAC (through grant no. FZ2022KF02), and by the National Natural Science Foundation of China (through grant no. U2133209).

References

[1] S. Sun, J. Hao, J. Yang, L. Zhou, and L. Ji, "Impacts of tandem configurations on the aerodynamic performance of an axial supersonic through-flow fan cascade," *Journal of Turbomachinery*, vol. 144, no. 4, article 041009, 2022.

[2] M. C. Johnson and E. M. Greitzer, "Effects of slotted hub and casing treatments on compressor endwall flow fields," *Journal of Turbomachinery*, vol. 109, no. 3, pp. 380–387, 1987.

[3] E. M. Greitzer, "Review-axial compressor stall phenomena," *Journal of Fluids Engineering*, vol. 102, no. 2, pp. 134–151, 1980.

[4] S. Sun, S. Chen, W. Liu, Y. Gong, and S. Wang, "Effect of axisymmetric endwall contouring on the high-load low-reaction transonic compressor rotor with a substantial meridian contraction," *Aerospace Science and Technology*, vol. 81, no. 10, pp. 78–87, 2018.

[5] S. Ma, W. Chu, H. Zhang, X. Li, and H. Kuang, "A combined application of micro-vortex generator and boundary layer suction in a high-load compressor cascade," *Chinese Journal of Aeronautics*, vol. 32, no. 5, pp. 1171–1183, 2019.

[6] J. Marty, L. Castillon, and P. Joseph, "Numerical investigations on the rotating stall in an axial compressor and its control by flow injection at casing," in *Proceedings of the ASME Turbo Expo 2022: Turbomachinery Technical Conference and Exposition*, Rotterdam, The Netherlands, 2022.

[7] G. R. Costello, R. L. Cummings, and G. K. Serovy, "Experimental investigation of axial-flow compressor stator blades designed to obtain high turning by means of boundary-layer suction," Tech. Rep. Archive & Image Library, National Advisory Committee for Aeronautics Collection, Washington, D. C., USA, 1952.

[8] K. R. Kirtley, P. Graziosi, P. Wood, B. Beacher, and H. W. Shin, "Design and test of an ultralow solidity flow-controlled compressor stator," *Journal of Turbomachinery*, vol. 127, no. 4, pp. 689–698, 2005.

[9] J. L. Kerrebrock, D. P. Reijnen, W. S. Ziminsky, and L. M. Smilg, "Aspirated compressors," in *Proceedings of the ASME 1997 International Gas Turbine and Aeroengine Congress and Exhibition*, Orlando, Florida, USA, 1997.

[10] S. A. Gbadebo, N. A. Cumpsty, and T. P. Hynes, "Control of three-dimensional separations in axial compressors by tailored boundary layer suction," *Journal of Turbomachinery*, vol. 130, no. 1, article 011004, 2008.

[11] P. Chen, *Investigations of Corner Separated Flow Loss Mechanism and Its Flow Control Techniques for Axial-Compressors*, Northwestern Polytechnical University, Xi'an, 2015.

[12] P. Chen, W. Qiao, K. Liesner, and R. Meyer, "Effect of segment end-wall boundary layer suction on compressor 3D corner separation," in *Proceedings of the ASME Turbo Expo 2015: Turbine Technical Conference and Exposition*, Montreal, Quebec, Canada, 2015.

[13] C. Gmelin, F. Thiele, K. Liesner, and R. Meyer, "Investigations of secondary flow suction in a high speed compressor cascade," in *Proceedings of the ASME 2011 Turbo Expo: Turbine Technical Conference and Exposition*, Vancouver, British Columbia, Canada, 2011.

[14] A. Godard, F. Bario, S. Burguburu, and F. Lebœuf, "Experimental and numerical study of a subsonic aspirated cascade," in *Proceedings of the ASME Turbo Expo 2012: Turbine Technical Conference and Exposition*, Copenhagen, Denmark, 2012.

[15] J. Ding, S. Wang, H. Xu, L. Cai, Z. Wang, and J. Shen, "The effect of aspiration configuration on aerodynamic performance in compound lean compressor cascades of gas turbines," *Applied Thermal Engineering*, vol. 130, pp. 264–278, 2018.

[16] S. Ma, W. Chu, X. Sun, Z. Guo, and S. Yan, "Effects of segmented layer suction and micro-vortex generator on a high-load compressor cascade performance," *Proceedings of the Institution of Mechanical Engineers, Part C: Journal of Mechanical Engineering Science*, vol. 235, no. 21, pp. 5309–5323, 2021.

[17] A. Hergt, R. Meyer, K. Liesner, and E. Nicke, "A new approach for compressor endwall contouring," in *Proceedings of the ASME 2011 Turbo Expo: Turbine Technical Conference and Exposition*, Vancouver, British Columbia, Canada, 2011.

[18] S. Sun, S. Wang, and S. Chen, "Design, modification and optimization of an ultra-high-load transonic low- reaction aspirated compressor," *Aerospace Science and Technology*, vol. 105, article 105975, 2020.

[19] S. A. Khalid, *The Effects of Tip Clearance on Axial Compressor Pressure Rise*, Massachusetts Institute of Technology, Massachusetts, 1995.